

THERMAL EVOLUTION OF COASTAL CALIFORNIA
WITH APPLICATION TO
HYDROCARBON MATURATION

Henry P. Heasler
Ronald C. Surdam

September 1985

Journal Article

WWRC-85-26

In

The American Association of Petroleum
Geologists Bulletin

Volume 69, No. 9

September 1985

Henry P. Heasler
Ronald C. Surdam
Department of Geology & Geophysics
University of Wyoming
Laramie, Wyoming

Thermal Evolution of Coastal California with Application to Hydrocarbon Maturation¹

HENRY P. HEASLER and RONALD C. SURDAM²

ABSTRACT

Coastal California has evolved through a series of plate tectonic interactions that significantly affected the geologic, thermal, and hydrocarbon maturation histories of the area. Numerical solutions for steady-state heat transfer are used to estimate temperature suppression resulting from plate subduction along coastal California, and to model thermal refraction within the Pismo basin. Numerical solutions for time-dependent heat transfer estimate the thermal effect of the passage of the Mendocino triple junction with consequent upwelling of asthenosphere. Thermal solutions vary for different areas along coastal California depending on the magnitude of the temperature suppression due to subduction, the geometry of the space into which the asthenosphere upwells, the time since passage of the triple junction, and the specific depositional history of each basin. Paleotemperatures are calculated for the Pismo basin, predicting that the basal 300 m of source rocks have generated hydrocarbons.

INTRODUCTION

Much of the petroleum production from onshore and offshore California originates in basins formed since the Oligocene (California Division of Oil and Gas, 1974; Hall, 1981; Isaacs, 1984). In these basins the Miocene Monterey Formation generally contains 1-5% organic carbon by weight, making it an excellent hydrocarbon source rock (Isaacs, 1981; Surdam and Stanley, 1981). Conventional maturation analysis using present-day geothermal gradients fails to predict the presence of mature source rocks in the relatively short time interval since the Oligocene (for examples see Heasler and Surdam, 1983; Isaacs, 1984). Previous workers have explained the presence of hydrocarbons as resulting from complete crustal attenuation and thermal subsidence (Turcotte and McAdoo, 1979; Heasler and Surdam, 1983), an increase in regional heat flow in the past (Kablanow and Surdam, 1983), or sediment burial and con-

sequent changes in the thermal conductivity of the sediments (Isaacs, 1984).

Difficulties exist with the various assumptions used in these maturation models. The model developed by Turcotte and McAdoo (1979) for the Los Angeles basin and used by Heasler and Surdam (1983) for the Pismo basin, in which a solution for a semi-infinite cooling half-space is used to estimate the thermal history, requires both the movement of large masses of 1,200°C material to the surface of the earth and only one-dimensional vertical heat transport. This model seems inadequate for the following reasons. (1) Hydrocarbon maturation patterns and heat-flow values vary from east to west and north to south across short distances (40 km) in California (California Division of Oil and Gas, 1973; Lachenbruch and Sass, 1980). This variation suggests that a semi-infinite half-space is not a valid approximation. (2) Many of the basins have enough structural relief to make horizontal heat transport important. (3) Although volcanoclastic rocks containing dikes and sills underlie the source rocks, it seems doubtful that the entire formation and everything beneath it would be raised to a temperature of 1,200°C by the volcanism. (4) These models assume a single time invariant thermal conductivity for the entire sedimentary sequence.

The maturation model presented by Kablanow and Surdam (1983) for the Huasna basin used heat-flow values proposed by Zandt and Furlong (1982), which overestimate the distribution of measured heat-flow values near the Pacific-North American plate boundary and underestimate the measured values more than 250 km south of Cape Mendocino. Kablanow and Surdam considered only vertical heat transport and neglected time-variant thermal parameters resulting from diagenetic and compaction histories.

Isaacs' (1984) hydrocarbon maturation model for coastal California considered only vertical heat transport and was based on a constant heat flow through time. However, coastal California has evolved through a changing thermal regime (Lachenbruch and Sass, 1980; Zandt and Furlong, 1982; Furlong, 1984; this paper). Although Isaacs' maturation model does not adequately represent the thermal history of the area, the paper does contain an important analysis of diagenetic reactions and the effect they may have on sediment thermal conductivities and compaction histories.

In this paper we attempt to formulate a realistic model for the thermal evolution of coastal California for use as a parameter in hydrocarbon maturation models for the area. The thermal models are checked by comparing calculated heat-flow values with published values and calculated maturation parameters with known maturation data from the Pismo basin.

© Copyright 1985. The American Association of Petroleum Geologists. All rights reserved.

¹Manuscript received, July 13, 1984; accepted, June 3, 1985.

²Department of Geology and Geophysics, University of Wyoming, Laramie, Wyoming 82071.

We thank Steve Boese for the analyses of organic carbon in Table 1 and many helpful discussions; Mike Lewan of Amoco Production Company for assistance in obtaining the data contained in Table 1; R. Kablanow, K. O. Stanley, and C. A. Hall for discussions of the Monterey Formation; Kevin Furlong and Peter Huntoon for insights into numerical modeling; and L. Crossey, D. Copeland, and A. Deiss for assistance in preparing the manuscript. The comments of James Helwig were helpful in revising the manuscript. This work was supported by NSF grant EAR-8207570 and a basic research grant from Texaco. The convective numerical modeling programs were developed by Heasler with funding from the Wyoming Water Research Center.

PLATE TECTONIC SETTING

The tectonic and thermal history of coastal California has been dominated for the last 30 m.y. by interactions between the North American, Farallon, and Pacific plates. Of major importance have been the effects of subduction and migratory triple junctions, and the opening of a slabless window. The following discussion is taken primarily from two papers by Dickinson and Snyder (1979a, b).

The Mendocino triple junction (MTJ) and Rivera triple junction (RTJ) were formed in the Oligocene when the ancestral East Pacific rise first encountered the North American plate. Until that time, the old Farallon plate had been subducted beneath the North American plate (Figure 1). After that encounter, there was a simultaneous migration of a fault-fault-trench triple junction (the MTJ) northward and a rise-trench-fault triple junction (the RTJ) southward along the Pacific-North American plate boundary (Figure 1). This broad boundary between the triple junctions, with its associated wrench tectonism, has been named the San Andreas transform (Wilson, 1965). The prior positions of the MTJ and the East Pacific rise crest are shown in Figure 2.

Associated with the migration of the triple junctions is the formation of a slabless window beneath the North American plate (Dickinson and Snyder, 1979b). Subduction ceased beneath the North American plate at the location where the ancestral East Pacific rise first impinged on the North American plate. Subduction of remnants of the Farallon plate (Juan de Fuca plate to the north, Rivera and Cocos plates to the south) continued north and south of the triple junctions. The relative motion of the plates resulted in the development of an area beneath the North American plate with no subducted oceanic lithosphere (Figure 3).

THERMAL EFFECTS OF SUBDUCTION AND THE MENDOCINO TRIPLE JUNCTION

The thermal effects of the plate tectonic history of California have been considered by various authors. Lachenbruch and Sass (1980) collected extensive thermal data for California and discussed the effect of frictional heating along the San Andreas fault system. They used a one-dimensional, analytic solution to approximate the thermal effect of asthenosphere upwelling into the slabless window of Dickinson and Snyder (1979b). Zandt and Furlong (1982) used a two-dimensional, time-dependent, finite difference model that approximated the thermal effect of asthenosphere upwelling into a rectangular window. Furlong (1984) used a two-dimensional, time-dependent, finite difference model to calculate the thermal effect of cooling asthenosphere emplaced in a trapezoidal region. The trapezoid is similar to the rectangle modeled by Zandt and Furlong, except one vertical side of the rectangle is given a dip of 30° to 45°. Furlong (1984) also considered the effect of subduction by initializing temperatures in the North American plate such that they were consistent with published surface heat-flow values for arc-trench gap regions.

All of the discussed models considered various constraints imposed by the plate tectonic history of coastal California. However, the thermal constraints were so generalized that the models were not applicable to the

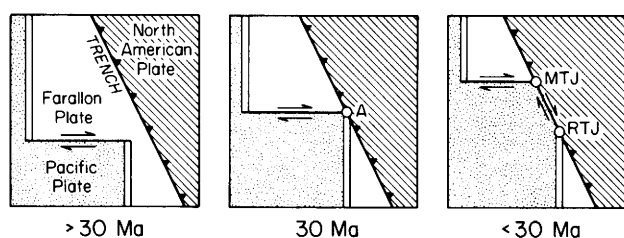


Figure 1—Generalized map showing relationship between North American, Farallon, and Pacific plates through time. Subduction of Farallon plate continued until approximately 30 Ma, when ancestral East Pacific rise crest (double line) impinged on North American plate at point A. Continued relative motions of plates generated San Andreas transform between northward migrating Mendocino triple junction (MTJ) and southward migrating Rivera triple junction (RTJ). Subduction of remnants of Farallon plate continued north of MTJ and south of RTJ. (Modified from Dickinson and Snyder, 1979b, their Figure 1.)

detailed analysis of specific basins. This is illustrated by the generally poor fit between modeled and measured heat-flow values for specific areas (e.g., see Zandt and Furlong, 1982, their Figures 3, 4).

The plate tectonic history of California imposes several constraints on the thermal evolution of the region. Subduction of the Farallon plate in the past and presently of the Juan de Fuca plate has caused a reduction in the temperatures within the arc-trench gap of the North American plate. Temperatures are suppressed in the arc-trench gap during subduction because cold oceanic lithosphere (the Farallon and Juan de Fuca plates) has moved beneath the North American plate forming a heat sink. The magnitude of the temperature suppression depends on the rate of subduction, the angle of subduction, and the thickness of lithosphere subducted. These parameters determine the amount of heat transferred due to mass transport (subduction).

Passage of the MTJ affects the thermal regime of the area in many ways. First, the oceanic lithosphere is no longer subducted beneath that portion of the North American plate (see Figure 3). This removes the cooling effect of the subducting oceanic lithosphere. Second, the formation of the slabless window creates a void into which hot (1,200°C) asthenospheric material moves and begins to cool. Third, the passage of the MTJ also puts the Pacific plate into contact with the North American plate. This movement and the dip of the subducted slab define the geometry of the window that the asthenosphere fills (Figure 3).

The temperature distribution and thickness of the Pacific plate and subducted oceanic plates vary with their ages. When the plates are initially formed at a ridge system, they are relatively thin and have a high temperature gradient. With time, the oceanic plates cool and consequently thicken (Turcotte and Oxburgh, 1969; Crough, 1975). The amount of temperature suppression due to subduction and the geometry of the base of the lithosphere after triple junction migration partially depend on the ages of oceanic lithosphere involved.

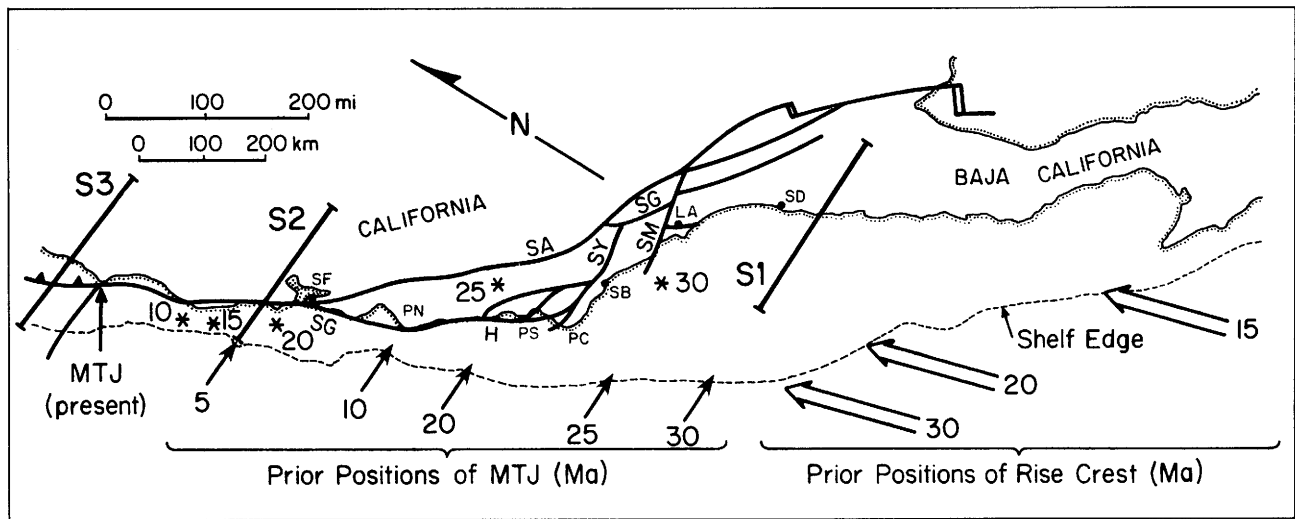


Figure 2—Map of coastal California showing positions of MTJ and East Pacific rise crest through time (after Dickinson and Snyder, 1979a, their Figures 8, 9). Asterisks represent estimated locations at various times of MTJ passage. Northward displacement of asterisks from prior positions of MTJ along continental slope is thought to represent Neogene slip of coastal slices between San Andreas fault, San Gregorio-Hosgri fault, and continental slope (Dickinson and Snyder, 1979a). Locations of subduction models are shown by S1, S2, and S3. Reference points are San Francisco (SF), Point Sal (PS), Point Conception (PC), Santa Barbara (SB), Los Angeles (LA), San Diego (SD), and Pinnacles (PN). Faults are San Andreas (SA), Santa Ynez (SY), San Gabriel (SG), Santa Monica-Malibu Coast (SM), Hosgri (H), and San Gregorio (SG) (after Hall, 1981).

THERMAL MODELING

Subduction

The effect of subduction lowering the temperature in the arc-trench gap was approximated with a steady-state, two-dimensional, finite difference model. Equation 1 describes steady-state conductive and convective heat transport:

$$\frac{\partial(K_x \partial T / \partial x)}{\partial x} + \frac{\partial(K_y \partial T / \partial y)}{\partial y} + \rho c (V_x \partial T / \partial x + V_y \partial T / \partial y) + A = 0, \quad (1)$$

where T represents temperature, K is thermal conductivity, ρ is the density of the convecting material, c is the specific heat of the convecting material, A is a heat source due to radioelement heat production, V is the velocity of the convecting material, and x and y subscripts are horizontal and vertical directions, respectively. This equation was solved numerically on the University of Wyoming's Cyber CDC 760 computer, using a method similar to that described by Kilty and Chapman (1980). (See Heasler, 1984, for additional details on the numerical modeling techniques.)

Input parameters for the model are a constant surface temperature, a basal heat flow, the thermal conductivity structure, and the thickness, velocity, density, and specific heat of the subducting oceanic lithosphere. The surface temperature was assumed constant at 10°C . A basal heat-flow value of $35 \times 10^{-3} \text{ W m}^{-2}$ was chosen as a reasonable value; it has also been used by Crough (1975), Lachenbruch and Sass (1980), Zandt and Furlong (1982), Furlong (1984), and others.

The thermal conductivity structure of the oceanic lithosphere was assumed constant at $2.9 \text{ W m}^{-1} \text{ K}^{-1}$ after Crough

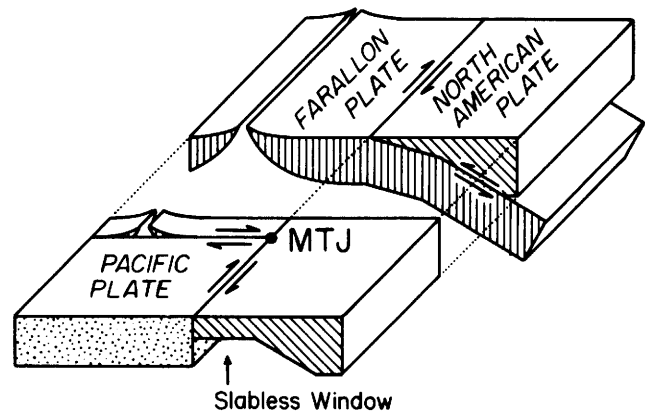


Figure 3—Diagrammatic representation of geometry of slabless window created by relative motions between North American, Farallon, and Pacific plates. (Modified from Zandt and Furlong, 1982, their Figure 2). Slabless window was created by right-lateral movement of North American plate off Farallon plate in area of Mendocino triple junction (MTJ) (Dickinson and Snyder, 1979b).

(1975), Black (1974), and others. This corresponds to the thermal conductivity of olivine basalt (Touloukian et al, 1981), approximately the rock type for lower oceanic crust (Christiansen and Salisbury, 1975). The thermal conductivity structure of the North American plate was assumed to be $2.5 \text{ W m}^{-1} \text{ K}^{-1}$ at the surface, which roughly corresponds to measured thermal conductivities reported by Sass et al (1971). In the North American plate, the thermal conductivity was assumed to increase to $2.7 \text{ W m}^{-1} \text{ K}^{-1}$ at a depth of 12 km and to $2.9 \text{ W m}^{-1} \text{ K}^{-1}$ at 21 km.

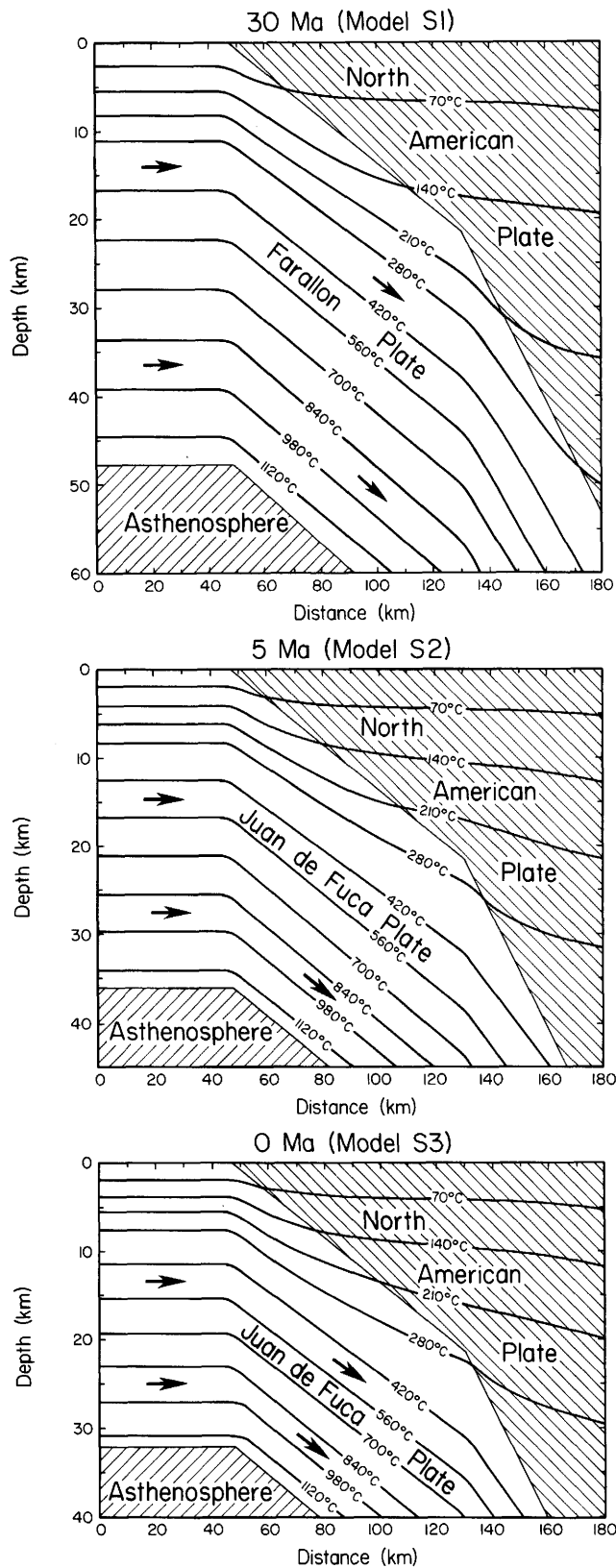


Figure 4—Results of numerical subduction models for Farallon and Juan de Fuca plates beneath North American plate at three locations along coastal California (see Figure 2 for locations). Subduction rates for models S1, S2, and S3 were 8, 3, and 3 cm year⁻¹, respectively (Dickinson and Snyder, 1979a). See text for discussion. Note vertical exaggeration.

Spreading and subduction rates were taken from Figure 6 of Dickinson and Snyder (1979a): spreading rates are 5 cm year⁻¹ for the Farallon plate and 3 cm year⁻¹ for the Juan de Fuca plate; subduction rates are 8 cm year⁻¹ for the Farallon plate and 3 cm year⁻¹ for the Juan de Fuca plate. Dickinson and Snyder (1979a) give a date of 5 to 7.5 Ma for the change in relative motion of the plates. Spreading rates are important because they define the age of oceanic lithosphere subducted. The thickness of the oceanic plate was calculated from the plate's age following the method of Crough (1975). In this calculation as well as the numerical solutions, 1,200°C was chosen to represent the temperature at the base of the lithosphere.

The density and specific heat used for the subducted slab were 3,300 kg m⁻³ and 1,000 J kg⁻¹ K⁻¹. These are typical values for an olivine basalt (Touloukian et al, 1981).

In the North American plate, an exponential decrease of radioactive heat-producing elements as proposed by Lachenbruch (1968) was included in the model. The resulting effect is to decrease temperatures at depth. The average value of 40 measurements of surface heat production for California from Lachenbruch and Sass (1980) is 1.5×10^{-6} W m⁻³. A characteristic depth over which heat production decreases cannot be well determined from the data of Lachenbruch and Sass. A characteristic depth of 10 km was chosen as a reasonable lower limit. No exponential decrease of heat-producing elements was included in modeling the oceanic lithosphere because of the small surface values of heat production (Black, 1974; Crough, 1975) and the consequent minor effect on the temperature structure.

The initial dip of a subducted slab is shallow, and then steepens to a final dip (Furlong et al, 1982). The dip of the slabless window as proposed by Dickinson and Snyder (1979b) is 30°. Furlong (1984) has shown that a dip of 30° to 45° is consistent with the observed heat-flow pattern in California. A final dip of 30° was chosen for this study. For simplicity in modeling, the initial shallow dip was taken to be a constant 15°. At a depth of 20 km, the dip was changed from 15° to 30° (Figure 4).

The geometry of subduction through time is poorly understood. Generally, as the age of the subducted plate decreases or as the convergence rate increases, the zone of shallow subduction of the plate decreases (Furlong et al, 1982). Also, the older the plate, the smaller the final subduction angle (Furlong et al, 1982). Given the uncertainties in the geometry of subduction, the effects of a subduction angle changing over time were neglected.

The results of three different applications of the subduction model are shown in Figure 4. Model S1 (Figure 4) is for a location just north of where the ancestral East Pacific rise impinged on California 30 Ma (see Figure 2 for location). At this time and location, the spreading rate was 5 cm year⁻¹, resulting in oceanic lithosphere about 20 m.y. old (from Dickinson and Snyder, 1979b, their Figures 5, 6; Dickinson and Snyder, 1979a, their Figure 6). Use of the method described by Crough (1975) results in a subducted oceanic lithosphere thickness of about 48 km. The subduction rate at this time was 8 cm year⁻¹ (from Dickinson and Snyder, 1979a, their Figure 6). Model S2 (Figure 4) is for the area just north of San Francisco at 5 Ma (see Figure 2 for

location). At 5 to 7.5 Ma, the relative motions of the plates changed (Dickinson and Snyder, 1979a). This resulted in oceanic lithosphere, which was about 36 km thick, being subducted at a slower rate of 3 cm year⁻¹. Model S3 (Figure 4) represents present-day subduction north of Cape Mendocino. Computed surface heat-flow values on the North American plate range from 35 to 42 × 10⁻³ W m⁻². This agrees well with the 40 × 10⁻³ W m⁻² used by Furlong (1984) as an initial condition to simulate subduction. The computed heat flows also agree well with the average of 42 × 10⁻³ W m⁻² for five measured values north of Cape Mendocino (Lachenbruch and Sass, 1980).

Lithospheric Upwelling

The thermal effect of the migrating MTJ and of the subsequent cooling of 1,200°C asthenosphere was approximated with a time-dependent, two-dimensional, finite difference model for conductive heat transport:

$$\partial(K_x \partial T / \partial x) / \partial x + \partial(K_y \partial T / \partial y) / \partial y + A = \rho c \partial T / \partial t. \quad (2)$$

The variables in equation 2 are the same as in equation 1, except ρ is density and c is specific heat of the rocks at every point in the model, and t refers to time. Equation 2 was solved numerically on the University of Wyoming's Cyber CDC 760 computer using the Livermore solver for ordinary differential equations (Hindmarsh, 1980).

Input parameters for the model included a basal heat flow, a surface temperature, the initial temperature distribution in the cross section of the model, thermal conductivities, density, and specific heat.

A surface temperature of 10°C was assumed for modeling purposes. The basal heat flow into the model was kept constant at 35 × 10⁻³ W m⁻², as in the subduction model. The thermal conductivity structure and heat-producing element distribution were similar to those used in the subduction models. The density and specific heat chosen resulted in a thermal diffusivity of 32 m² year⁻¹, a commonly accepted value. (Thermal diffusivity is defined as thermal conductivity divided by density and specific heat; it is presently a poorly known constraint in thermal modeling.)

Results of the time-dependent model are sensitive to the initial temperature distribution. The initial temperature distribution for different areas in the North American plate were taken from the subduction models. The initial temperature distribution in the Pacific plate varied with the age of the plate. When the ancestral East Pacific rise first impinged on the North American plate (Figure 2), the Pacific plate would have been very thin. As a result, the 1,200°C asthenosphere would have been brought to a shallow depth under the Pacific plate. As time continued, the Pacific plate cooled and thickened. Thus, the North American plate was coming into contact with a cooler and thicker Pacific plate as the MTJ migrated. This effect was included in the initial conditions of the time models by calculating a thickness for the Pacific plate after Crough (1975). The calculated thickness was based on the time since the impingement of the ancestral East Pacific rise. A linear temperature gradient is assumed to have existed within the Pacific plate.

An additional constraint on the initial temperature distribution of the time-dependent models is the geometry of the

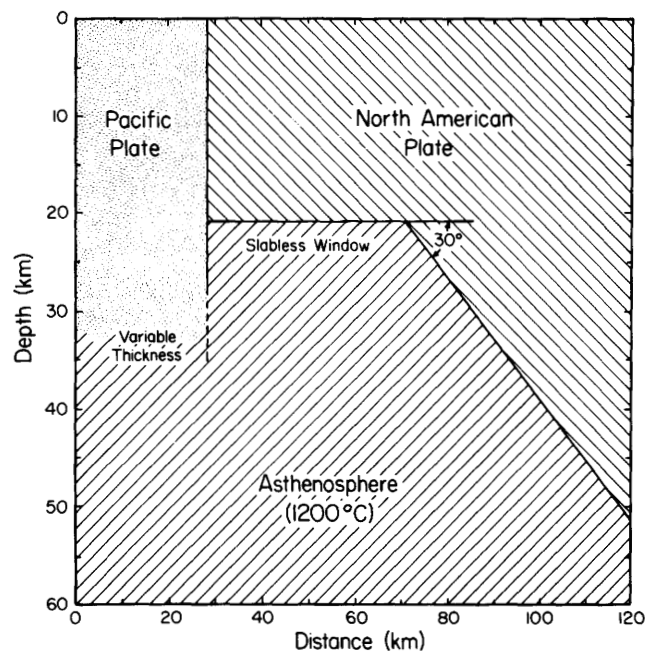


Figure 5—Initial geometry of North American plate, Pacific plate, and slabless window used in time-dependent numerical models. Note vertical exaggeration.

slabless window created by the migrating MTJ. The geometry of the window is important because it defines the area into which 1,200°C asthenosphere can move. Lachenbruch and Sass (1980) considered the thickness of the North American plate above the window in their one-dimensional model. They found that a North American plate thickness of 20 km resulted in a good correspondence between calculated and observed heat-flow values. Zandt and Furlong's (1982) discussion of the two-dimensional geometry of the window was based on the results of teleseismic delay studies and thermal models. They used a rectangular window that was 20-30 km beneath the North American plate and 80-100 km wide. Furlong (1984) modified the shape of the window by including the effect of a 30°-45° dip of the window toward the North American plate. The geometry of the window used in the present study is shown in Figure 5 and is similar to the geometries used by Zandt and Furlong (1982) and Furlong (1984). The area of mass in the North American plate above the slabless window (Figure 5) is the same as the area of mass above the 15° dip in the subduction model (Figure 4).

For the asthenosphere, Lachenbruch and Sass (1980) used a 3°C km⁻¹ gradient. Such a small gradient in the asthenosphere would have little effect on temperatures in the upper 6 km of the crust where sedimentary basins have formed. For simplicity in modeling, a constant temperature of 1,200°C was used in the present study to represent the asthenosphere.

Results from the time-dependent models are shown in Figures 6-9. Figure 6 shows temperature cross sections at various times for a location near Point Conception (see Figure 2 for location). Figure 7 illustrates the variation of surface heat flow in the area near Point Conception as a function of both time and distance across the Pacific-North

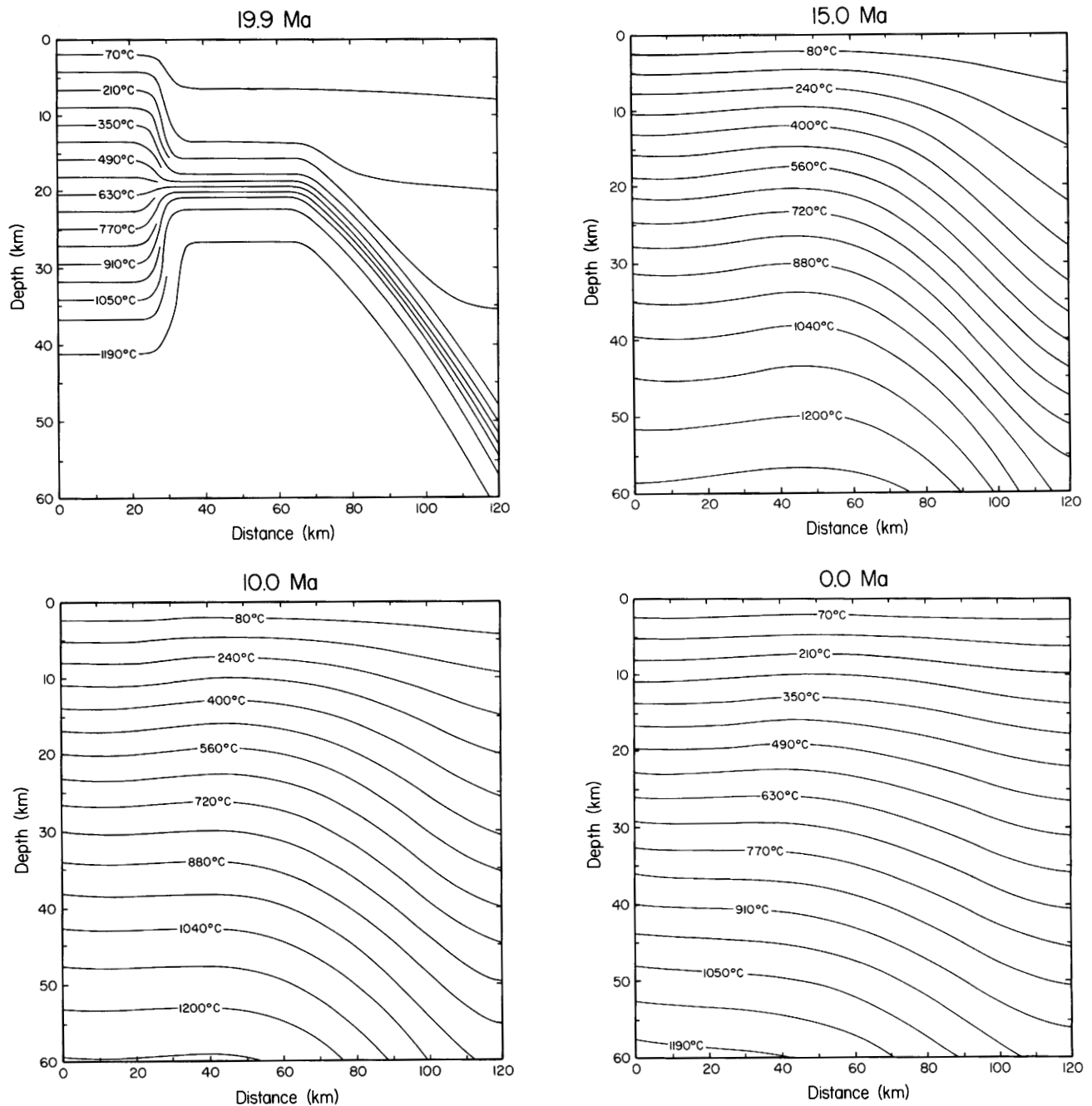


Figure 6—Results of time-dependent numerical model for region near Point Conception. Passage of Mendocino triple junction is assumed to have occurred approximately 20 Ma. See text for discussion. Note vertical exaggeration.

American plate boundary. Figures 6 and 7 show the thermal pulse caused by the 1,200°C asthenosphere emplacement reaching the surface 3-5 m.y. after MTJ migration. These figures also illustrate the magnitude of the thermal anomaly varying with both time and distance from the plate boundary. Figure 8 illustrates the variation of heat flow through time for locations near Point Conception, the Pinnacles, and San Francisco. Figures 7 and 8 show that the presently observed high heat flows in north-central California result from the recency of the thermal event caused by the migrating MTJ and an increase in the

magnitude of the thermal anomaly northward along coastal California.

An important check on time-dependent models is to compare measured surface heat-flow values with those predicted by the models. As shown in Figure 9, the computed values are similar to the measured values from Lachenbruch and Sass (1980). Problems that may affect the modeled results are as follows: (1) the possibility of 305 km of Neogene right-slip movement along the San Andreas transform (Graham and Dickinson, 1978; Stanley and Surdam, 1984), thereby moving portions of the North American

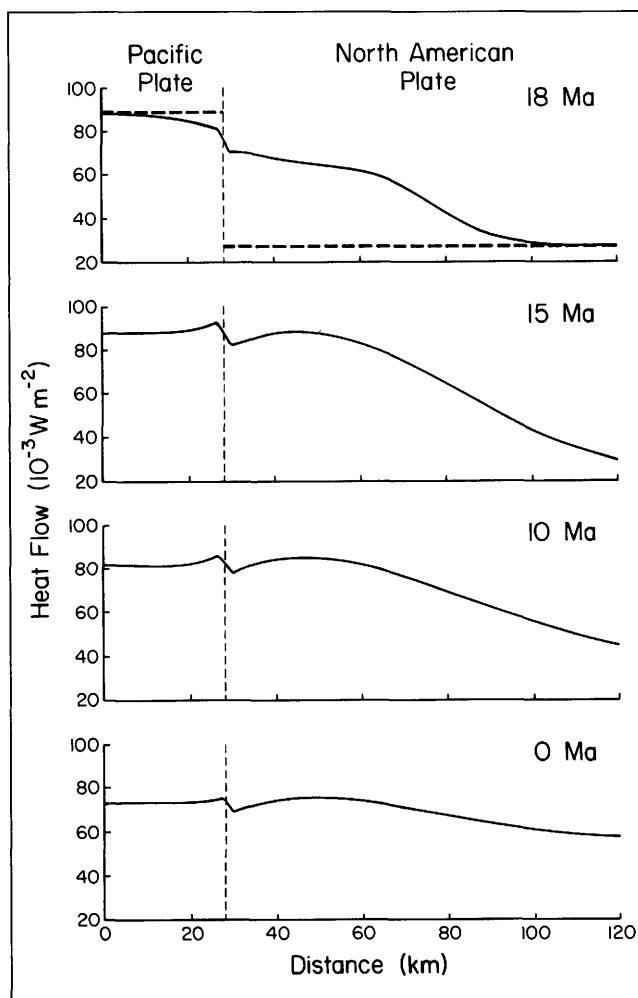


Figure 7—Surface heat flow as a function of time and position for region near Point Conception. Initial heat flow at 20 Ma is shown by heavy dashed lines on 18 Ma graph. Change in heat flow at Pacific–North American plate boundary results from thermal conductivity differences between plates. Temperatures are continuous across boundary (see Figures 5, 6).

plate into different thermal regimes; (2) the complex tectonic style along the Garlock fault zone with possible rotation of the Transverse Ranges into their present position (Hall, 1981); (3) the highly localized effect of frictional heating along faults of the San Andreas transform (Lachenbruch and Sass, 1980); and (4) the effect of the release of latent heat as the asthenosphere cools. The ability of the time-dependent models to match the present-day heat-flow distribution suggests that these effects are second order and that the models are a good representation of the thermal history of coastal California.

Refraction

The effect of heat refraction was estimated with the two-dimensional, steady-state, finite difference model described previously. In the Pismo basin, the known geologic structure was incorporated into the model by estimating rock thermal conductivities. The basal heat-flow for this shallow

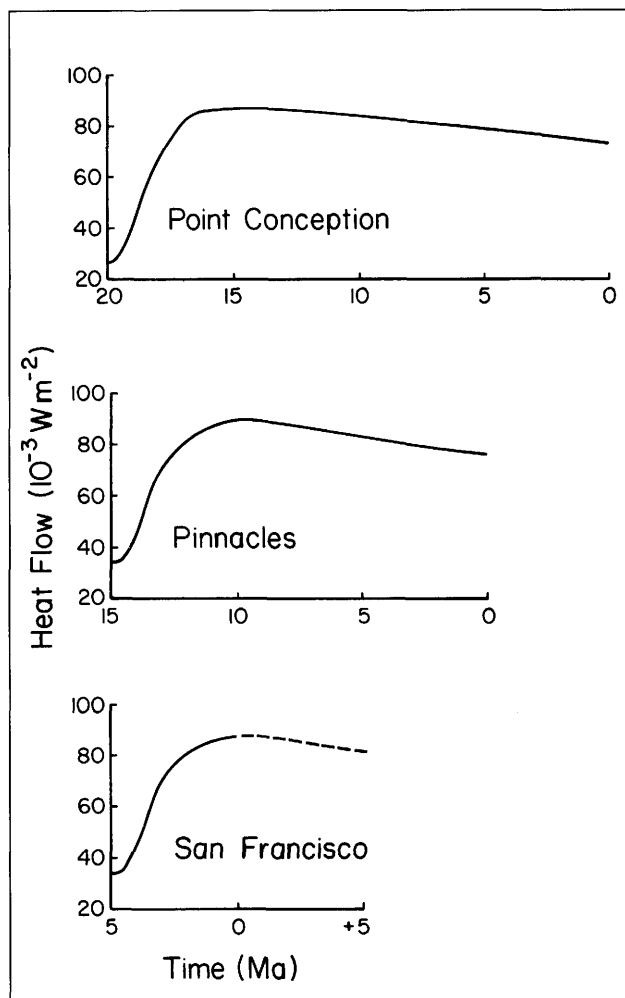


Figure 8—Surface heat flow as a function of time for three locations along coastal California. Locations for three graphs are on North American plate 15 km east of Pacific–North American plate boundary. Note that graph for San Francisco area extends 5 m.y. into future (dashed curve).

model (5 km) was taken from results of the time-dependent models. The geologic and thermal conductivity structure of the basin was estimated through time in order to place limits on refraction and its effect on the temperature structure of the basin. The results of this modeling are discussed in more detail in the following section.

HYDROCARBON MATURATION MODELING

The regional thermal history is but one input parameter of the hydrocarbon maturation model for a basin. Other important parameters include type of source rock, subsidence history, depositional rates, geometry of the basin through time, and types of sediments in the basin, including their diagenetic and compaction histories. The Pismo basin was chosen for this study because a large amount of such data exists for the basin and nearby areas.

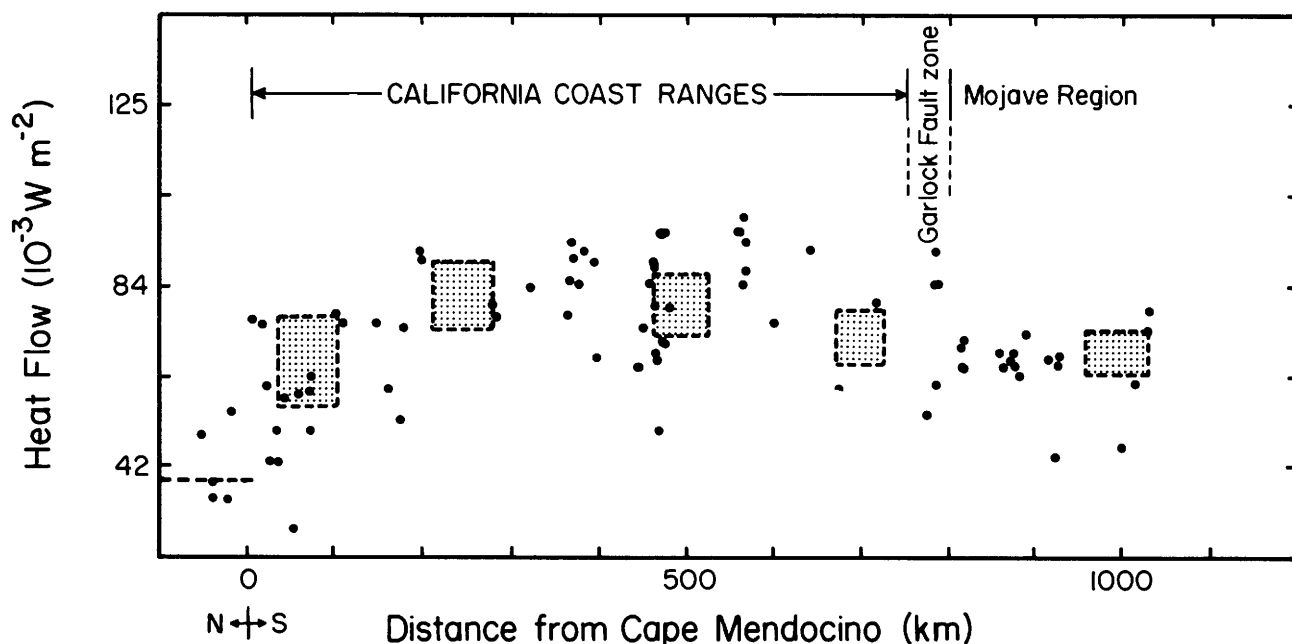


Figure 9—Modeled heat-flow values (dashed horizontal line and stippled areas) shown with measured heat-flow values (solid circles) from Lachenbruch and Sass (1980). North of Cape Mendocino, modeled heat-flow results (dashed horizontal line) are from subduction model S3. South of Cape Mendocino, heat-flow results (stippled area surrounded by dashed lines) are from time-dependent numerical models. Heat-flow results from time-dependent models vary both with time since passage of Mendocino triple junction and distance from Pacific-North American plate boundary (see Figures 7, 8, and text). Consequently, ranges of modeled heat-flow values are shown as areas, rather than single points.

Geology of Pismo Basin

The Pismo basin is located within a tectonic block bounded on the northeast by the West Huasna fault, on the south by the Santa Maria River fault, on the west by the Hosgri fault (Figures 2, 10), and is just north of the Santa Maria basin. Hall (1981) showed that both the Santa Maria and Pismo basins are pull-apart structures. The Pismo basin is a relatively simple fold (Figure 11) that served as a depositional basin during the Miocene and Pliocene.

In the Pismo basin, the Miocene Obispo Formation overlies a thin section of the Miocene Rincon formation. Rincon formation unconformably overlies the Mesozoic Franciscan Formation in most parts of the basin. Disconformably above Obispo Formation is the Miocene Monterey Formation, which is in turn overlain by the Miocene-Pliocene Pismo Formation (Hall, 1973a, b).

The Obispo Formation ranges from 500 to 1,000 m thick throughout most of Pismo basin. The formation consists mainly of rhyolitic debris in the form of tuff and tuffaceous mudstone and siltstone. Near the source of the volcanic debris—a series of volcanic highs along the western margin of the basin—the Obispo Formation consists of various rock types such as flows, sills, intrusive plugs, breccia, and tuff. The Obispo Formation has been dated at 15.3 to 16.5 Ma (Turner, 1970). The largely pyroclastic Obispo Formation and equivalent volcanic units occur along a trend 140-200 km long in the southern Coast Ranges of California. These volcanic rocks were intruded, extruded, and ejected into a continental submarine margin along the San Luis Obispo transform (Hall, 1981).

In this area Monterey Formation is up to 1,500 m thick and contains three significant lithofacies: siliceous, carbonate-phosphatic, and siliciclastic facies (Surdam and Stanley, 1981). The siliceous facies contains 1-5 wt. % organic carbon, and the carbonate-phosphatic facies contains up to 18

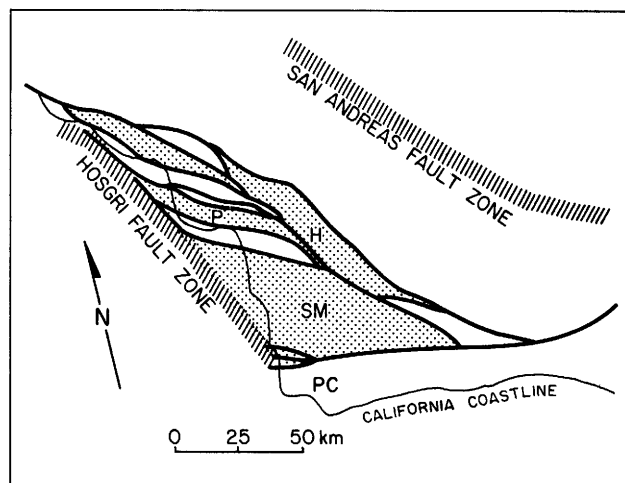


Figure 10—Simplified map showing tectonic setting of Pismo basin (P). Pismo basin is separated from Huasna basin (H) by West Huasna fault and from Santa Maria basin (SM) by Santa Maria River fault. Major tectonic element to west is Hosgri fault system. Stippled areas are depositional basins. PC refers to Point Conception. (Modified from Hall, 1981.)

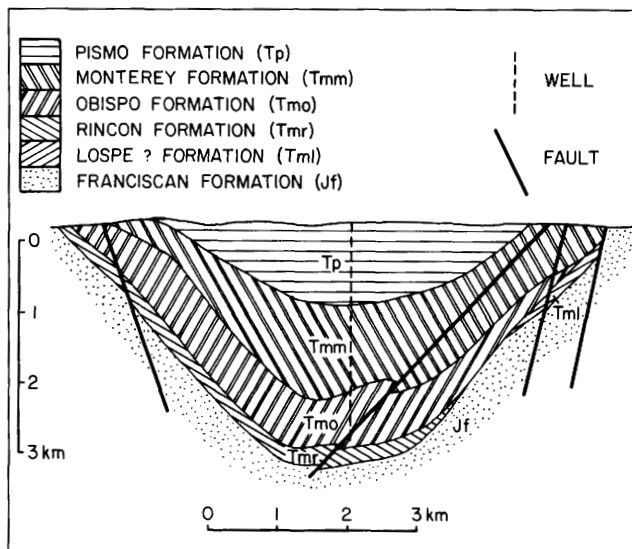


Figure 11—Schematic cross section through Pismo basin. Note that Monterey Formation thins on limbs of fold. Names are from Hall (1973a, b).

wt. % organic carbon (for more details see Surdam and Stanley, 1981).

The Miocene-Pliocene Pismo Formation is up to 1,000 m thick and consists of diatomaceous shale, siltstone, and sandstone. Along the western edge of the basin, adjacent to the San Miguelito fault, this formation overlies the Monterey Formation in angular discordance. However, in the center of the basin the Pismo Formation conformably overlies the Monterey Formation with no evidence of a break in deposition. The unconformity between the two formations along the western margin of the Pismo basin is attributed to activity along the San Miguelito fault during deposition and possibly to sea level changes (Stanley and Surdam, 1984). This tectonic activity at the margins contrasts with the more constant depositional history in the center of the basin.

Source Rock Character

The Miocene Monterey Formation has outstanding source rock potential. Total organic carbon values are high, ranging between 1.3 and 4.7 wt. % (Table 1). Organic sulfur values for some kerogens in the Monterey Formation are greater than 9 wt. % (Orr, 1984). In Pismo basin, both the siliceous and carbonate-phosphatic lithofacies of the Monterey Formation have outstanding source rock potential.

An effective way to determine the kerogen type contained in the Monterey Formation is to plot atomic H/C and O/C ratios from Table 1. Figure 12 shows that more than 70% of the data falls within a type II kerogen (exinite) field. Hunt (1979) specifies H/C ratios of 0.3 to 1.4 and O/C ratios of 0.02 to 0.2 for type II kerogen. The data from Table 1 are within these ranges with H/C ratios of 0.83 to 1.32 and O/C ratios of 0.08 to 0.14.

Subsidence History

Scant data exist for the absolute ages of formations in the Pismo basin, thus making reconstruction of subsidence

curves highly speculative. Rapid subsidence could be caused by a cooling half-space, as proposed by Turcotte and Ahern (1977) and applied to the Los Angeles basin by Turcotte and McAdoo (1979) and to Pismo basin by Heasler and Surdam (1983). However, as previously discussed, the cooling half-space model is inadequate for Pismo basin. The true subsidence history may be a combination of thermal subsidence imposed on lithospheric flexure. The effective elastic thickness of the lithosphere in this area has likely been modified by fault penetration and high temperatures. A linear subsidence model would underestimate the sediment depths at a given time when compared to a simple thermal subsidence model (e.g., see Heasler and Surdam, 1983, their Figures 8, 9). Therefore, as a first approximation, we have assumed a constant deposition rate for each formation, realizing that hydrocarbon maturation may be underestimated by the model.

The diagenetic and compaction history of the Monterey Formation has been summarized in Isaacs (1984). Following the method of Isaacs, thermal parameters for the Monterey Formation were calculated (Table 2). Transitions from opal A to opal CT to quartz in the Monterey Formation are primarily temperature dependent (Murata et al, 1977). Thus, changes in thermal conductivity corresponding to these transitions are also temperature dependent.

Depositional rate calculations were based on the present thickness of the Monterey Formation in the center of the Pismo basin. The depositional rate used in the modeling was constant from 16 to 7 Ma (dates after Surdam and Stanley, 1981) at 450 m m.y.^{-1} . This rate assumes an original porosity of 70%. Isaacs (1983) stated a range of 45 to 250 m m.y.^{-1} at an original porosity of 80% with deposition from approximately 18 to 6 Ma.

Little is known about the porosity and thermal conductivity structure for the Pismo Formation. Thermal parameters shown in Table 3 for the Pismo Formation were calculated assuming an exponential decrease in porosity (after Steckler and Watts, 1978). The depositional rate used for the Pismo Formation at the center of the Pismo basin was 250 m m.y.^{-1} , assuming a depositional porosity of 50%. Deposition was assumed to have occurred from approximately 7 to 2 Ma (Surdam and Stanley, 1981). Isaacs (1983) stated depositional rates for the Sisquoc Formation (approximately equivalent to the Pismo Formation) of $375\text{--}1,850 \text{ m m.y.}^{-1}$, for an original porosity of 80%.

The subsidence and maturation histories must also include the effects of the deposition and removal of up to 400 m of conglomeratic Paso Robles Formation during the Pleistocene (Hall, 1973a; 1983, personal communication).

Subsidence and thermal histories of the Monterey Formation can be calculated using the thermal conductivity data in Tables 2 and 3, the deposition rates discussed above, and the modeled heat-flow through time from Figure 7. Table 4 lists the calculated temperature history for these two sedimentary horizons.

The temperature calculations are for the center of the Pismo basin and, as a first approximation, assume only vertical heat transport. To assess the effect of two-dimensional heat transport, finite difference models were used to estimate the effects of differing sedimentary geometries and

Table 1. Thermal Evolution Data for Monterey Formation in Pismo Basin

Sample No.*	Organic Carbon (wt. %)	Atomic H/C	Atomic O/C	Volatile HC (S ₁)**	Generated HC (S ₂)**	Transformation Ratio**
NSB-5	ND†	1.32	0.14	IS††	IS	
NSB-7	ND	1.30	0.12	IS	IS	
PO-24	ND	1.30	0.11	IS	IS	
N-613	1.9	1.20	0.12	7.59	127.29	0.06
N-771	1.7	1.23	0.11	5.98	54.69	0.10
N-799	3.0	1.19	0.12	4.91	96.27	0.05
N-866	1.5	1.23	0.12	3.69	62.12	0.06
N-933	2.1	1.30	0.11	4.26	68.77	0.06
N-1147	2.3	0.96	0.11	2.64	46.54	0.05
E-1375	1.3	1.21	0.11	5.28	61.28	0.08
E-1449	3.6	0.83	0.11	3.32	7.43	0.31
E-1519	1.4	1.11	0.12	3.53	65.27	0.05
E-1576	3.1	0.94	0.14	2.95	59.38	0.05
E-1698	2.3	ND	ND	10.12	26.36	0.28
E-1770	3.1	1.18	0.11	IS	IS	
E-1870	4.7	0.95	0.11	3.77	19.51	0.16
E-1950	3.6	1.13	0.09	5.15	89.85	0.05
E-2111	2.3	1.13	0.08	IS	IS	
E-2113	1.7	ND	ND	5.83	64.85	0.08

*Outcrop samples include NSB and PO numbers. N numbers are samples from the Holmes 1 well, Sec. 6, T32S, R13E, San Luis Obispo County, California. E numbers are samples from the Elberta well, Sec. 5, T32S, R13E. Numbers after N or E refer to depth in meters.

** See text for discussion.

†ND = not determined.

††IS = insufficient sample.

thermal conductivities. Two examples of these calculations are shown in Figure 13. A 10-20% decrease in temperatures due to refraction existed from 0 to 7 Ma. From 7 to 16 Ma, the refraction effect decreases to zero. Temperatures resulting from a 20% refraction correction (an upper limit to the correction) are also shown in Table 4.

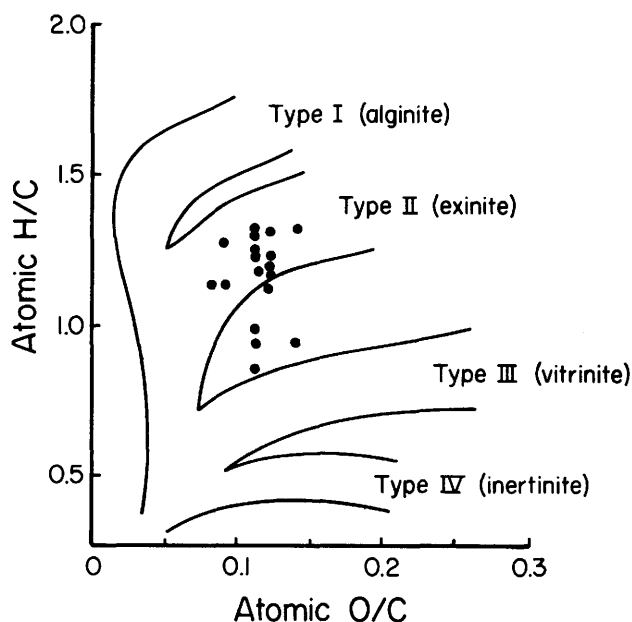


Figure 12—H/C vs. O/C plot (after Waples, 1981) for kerogen from Monterey Formation. Data are from Table 1.

Maturation Models

Given the temperature history of sediments as shown in Table 4 and Figure 13, kerogen maturity can be calculated by either Lopatin's method as described by Waples (1981) or the method of Tissot and Espitalié (1975).

Lopatin's method of predicting hydrocarbon maturation assumes that a time and temperature interrelationship determines the maturity of kerogen. Thus, a high temperature over a short time interval may have the same maturation effect as a lower temperature over a longer time interval. Lopatin's method assumes that, for every 10°C temperature increase, the maturation rate increases by a factor of 2.

To calculate the maturity of a kerogen by Lopatin's method, equation 3 is used:

$$TTI = \sum 2^m \text{time}_m, \quad (3)$$

where TTI is the calculated measure of maturity (the time-temperature index), time_m is the length of time (in million years) spent by the kerogen in the m^{th} temperature interval, and 2^m is the temperature factor, shown in Table 5. Waples (1981) correlated a TTI of 15 with the onset of oil generation (entrance into the liquid oil window) and a TTI of 75 with peak oil generation.

Results of TTI calculations are listed in Table 4 for two sedimentary horizons in the Monterey Formation. Refraction corrections to temperatures make a substantial difference in TTI values. TTI values for the base of the Monterey Formation range from 35 (well into the liquid oil window), without the refraction correction, to 8 (immature), with the refraction correction. At a horizon 300 m above the base of

Table 2. Thermal Parameters for Monterey Formation

	Opal A		Opal CT		Quartz
Porosity (%)	70		35		10
Temperature of transition (°C)		50		80	
Thermal conductivity (W m ⁻¹ K ⁻¹)	0.9*		1.3		1.6**

*Agrees with values reported by Erickson (1973) for sea-floor sediments.

**Agrees with values from Benfield (1947).

the formation, TTI values range from 14 (no refraction correction) to 3 (corrected).

A difficulty with Lopatin's method is that it does not directly consider the kerogen type in the source rocks. Thus, it underestimates the amount of hydrocarbons generated from a kerogen that matures at lower temperatures. Also, the correlation of a TTI of 15 with the onset of oil generation is based on correlations with oil generation in many different types of basins. Such correlations may not be directly applicable to the evolution of kerogens in the Pismo basin.

Tissot and Espitalié (1975) considered variations between types of kerogen and calculated a transformation ratio—a measure of kerogen maturity—which can be compared to laboratory measurements of the transformation ratio. In the Tissot and Espitalié method, the mass fraction of kerogen (x_i) is related to the activation energy (E_i), the universal gas constant (R), the absolute temperature (T), the time (t), and a rate constant (A_i), by the maturation equation:

$$dx_i = -x_i A_i \exp(-E_i/RT) dt. \quad (4)$$

The kinetic parameters determined by Tissot and Espitalié (1975) for a type II kerogen are shown in Table 6. The only time-varying parameter in equation 4 is temperature.

Using the temperatures listed in Table 4 and the parameters listed in Table 6 for a type II kerogen, equation 4 can be numerically integrated. The numerical integration results in a value for x_i for a given time-temperature history.

The transformation ratio, defined by Tissot and Welte (1978) as the ratio of kerogen already transformed to the genetic potential of the kerogen, is stated mathematically by the expression:

$$(\Sigma x_{i_0} - \Sigma x_i) / (\Sigma x_{i_0}), \quad (5)$$

where the genetic potential of a kerogen (x_{i_0}) is the total amount of hydrocarbons that can be produced by that type of kerogen for a specific activation energy (see Table 6).

The computed transformation ratio is similar to the transformation ratio measured in the laboratory by pyrolysis, in which organic material is thermally decomposed in a pyroprobe and detected in two stages (Tissot and Welte, 1978) (Table 1). The S1 stage represents short-chained hydrocarbons (less than C₁₅) that boil at less than 250°C. This stage is generally considered to represent generated hydrocarbons. The second stage, S2, includes long-chained hydrocarbons and immature kerogen that decomposes between 250° and 600°C. The transformation ratio is calculated from these two stages by equation 6:

$$S1/(S1 + S2). \quad (6)$$

As kerogen matures, the transformation ratio should increase because generated hydrocarbons (S1) increase.

Laboratory pyrolysis data must be interpreted with care, as discussed by Kablanow and Surdam (1983). Problems may exist because the S1 stage measures only short-chained hydrocarbons presently in the sample. Some short-chained hydrocarbons may be lost prior to measuring the sample because of their volatility. Additionally, some generated hydrocarbons may be greater than C₁₅, which would result in larger S2 and smaller S1 stages. Both effects would decrease the measured transformation ratio. The results of laboratory pyrolysis data for the Pismo basin are listed in Table 1.

It is uncertain how much oil of biochemical origin is retained in samples from Pismo basin that would consequently be included in the S1 pyrolysis measurement. In this paper, biochemical oil includes any oil not formed by kerogen catagenesis involving activation energies of at least 10 kcal/mole. This oil would include hydrocarbons generated at low temperatures (generally less than 80°C) by low activation energies and any oil that may have been present during sediment burial.

Because of the uncertainty in the amount and retention of biochemical oil, the calculated transformation ratios for a type II kerogen were computed by two methods. The first

Table 3. Thermal Parameters for Pismo Formation

Depth (m)	0	300	600	900	1,200	1,500	1,800	2,100
Porosity* (%)	50	44	38	33	29	25	22	19
Thermal conductivity** (W m ⁻¹ K ⁻¹)	1.7	2.0	2.2	2.5	2.7	3.0	3.1	3.4

*Assuming an exponential decrease in porosity due to compaction. Calculated following the method of Steckler and Watts (1978). Porosity observed at the present time would be equivalent to porosity achieved at the greatest depth the sediment had obtained.

**Calculated following the method of Woodside and Messmer (1961). Pore spaces are assumed to be water filled. This formation in the area of the Pismo basin is assumed to be a sandstone containing 70% quartz and 30% feldspar.

Table 4. Thermal History of Two Sedimentary Horizons of Monterey Formation in Pismo Basin

Time (Ma)	Base of Monterey				300 m Above Base of Monterey			
	Uncorrected		Corrected*		Uncorrected		Corrected*	
	T (°C)	TTI	T (°C)	TTI	T (°C)	TTI	T (°C)	TTI
16	10	0.0020	10	0.0020				
15	51	0.0313	51	0.0313	23	0.0039	23	0.0039
14	65	0.0625	64	0.0625	43	0.0078	42	0.0078
13	78	0.125	74	0.125	54	0.0313	51	0.0313
12	87	0.25	81	0.25	69	0.0625	64	0.0625
11	95	0.5	86	0.25	80	0.25	72	0.125
10	103	1	91	0.5	87	0.25	77	0.125
9	109	1	93	0.5	93	0.5	79	0.125
8	115	2	95	0.5	100	1	83	0.25
7	122	4	98	0.5	100	1	80	0.25
6	124	4	99	0.5	109	1	87	0.25
5	124	4	99	0.5	109	1	87	0.25
4	125	4	100	1	110	2	88	0.25
3	125	4	100	1	111	2	89	0.25
2	125	4	100	1	111	2	89	0.25
1	127	4	102	1	113	2	90	0.5
0	117	2	94	0.5	100	1	80	0.25
Total TTI		35		8		14		3
Transformation ratio for type II kerogen**		0.43		0.09		0.17		0.04
Transformation ratio for type II kerogen with biochemical hydrocarbon**		0.46		0.13		0.21		0.09
Transformation ratio for Phosphoria shale (sulfur-rich type II kerogen)†		1.00		0.28		0.73		0.04

*To correct for thermal refraction, temperatures have been reduced 20% from 0 to 7 Ma. From 8 to 15 Ma the correction due to refraction was assumed to linearly decrease to 0.

**Kinetic parameters from Tissot and Espitalié, 1975.

†Kinetic parameters from Lewan, 1985.

method, as previously discussed, considers only the mass fraction of kerogen converted to petroleum. The second method considers the effect of hydrocarbons of biochemical origin (values from Tissot and Espitalié, 1975) by adding the amount of those hydrocarbons (Y_o) into both the numerator and denominator of the calculated transformation ratio:

$$(Y_o + \sum x_{i0} - \sum x_i) / (Y_o + \sum x_{i0}) \quad (7)$$

Results of these two methods are listed in Table 4 for two sedimentary horizons in the Monterey Formation.

A third method for calculating hydrocarbon maturity is a modified Tissot and Espitalié technique. Hydrocarbon maturity is calculated as previously described, except a single activation energy of 42.7 kcal mole⁻¹ and a rate constant of $4.31 \times (10^{-17} \text{ years})^{-1}$ are used. These values are from Lewan's (1985) hydrous pyrolysis measurements of sulfur-rich kerogen in the Phosphoria shale. Some Monterey For-

mation kerogens are known to contain greater than 9 wt. % organic sulfur (Orr, 1984). The Phosphoria shale studied by Lewan (1985) also contained 9 wt. % organic sulfur. Both Lewan and Orr hypothesized that the greater the amount of organic sulfur incorporated into the matrix of a type II kerogen, the lower the thermal stress necessary for oil generation. Thus, we have approximated the kinetic parameters of a sulfur-rich kerogen of the Monterey Formation by using Lewan's kinetic values for the Phosphoria shale.

Transformation ratios calculated for a sulfur-rich type II kerogen are shown in Table 4 for two sedimentary horizons in the Monterey Formation. Figure 14 illustrates the difference in basal Monterey Formation maturity as a function of time for the Tissot and Espitalié and modified Tissot and Espitalié methods.

A transformation ratio of 0.10 to 0.45 has been correlated with the liquid oil window (see Tissot and Welte, 1978, p. 454). Calculated transformation ratios for a type II

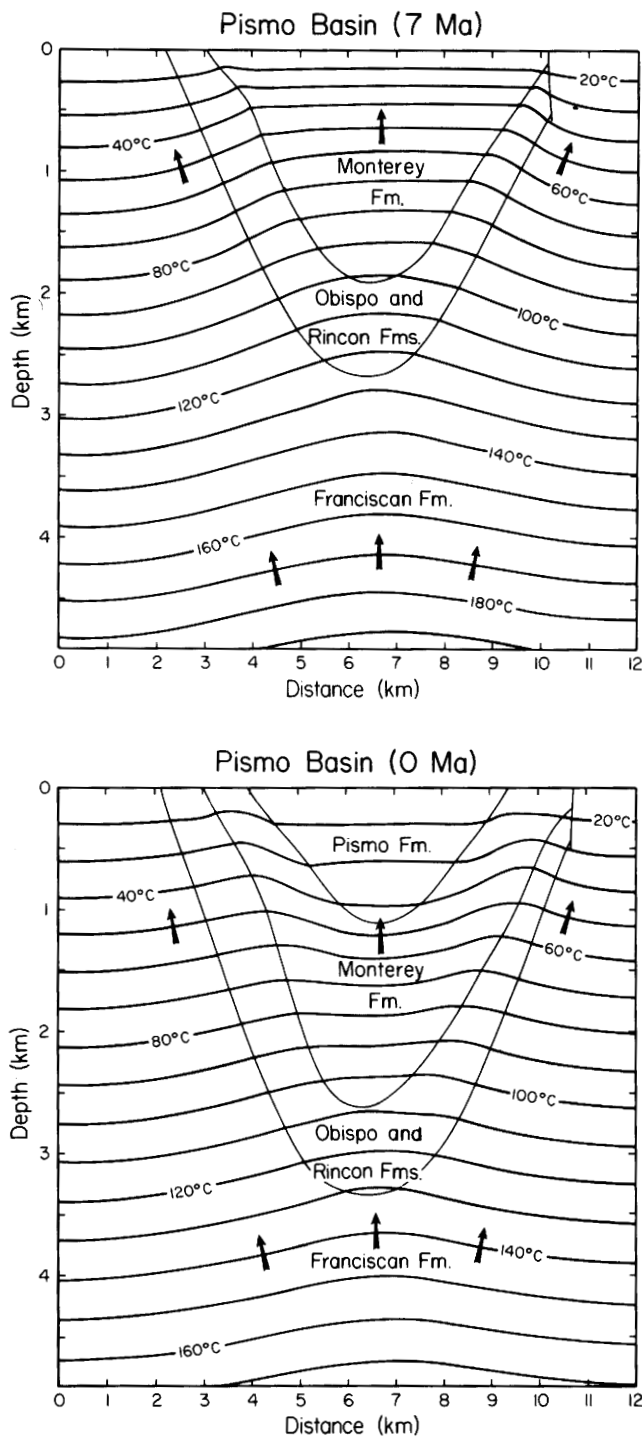


Figure 13—Examples of numerically modeled effects of thermal refraction on sediment temperatures in Pismo basin. Arrows indicate direction of heat transport. Note vertical exaggeration.

kerogen range between 0.09 and 0.13 for the corrected temperatures at the base of the Monterey Formation and between 0.04 and 0.09 for the corrected temperatures at 300 m above the base (see Table 4). Transformation ratios calculated for corrected temperatures using kinetic values for the Phosphoria shale (Lewan, 1985) range between 0.28 for the basal Monterey Formation and 0.04 at 300 m above the

Table 5. Temperature Factors for Lopatin's Maturation Method*

Temperature Interval (°C)	m	Temperature Factor
50-60	-5	$2^{-5} = 0.0313$
60-70	-4	$2^{-4} = 0.0625$
70-80	-3	$2^{-3} = 0.125$
80-90	-2	$2^{-2} = 0.25$
90-100	-1	$2^{-1} = 0.5$
100-110	0	$2^0 = 1$
110-120	1	$2^1 = 2$
120-130	2	$2^2 = 4$
.	.	.
.	.	.
...	m	2^m

*After Waples (1981).

base. The calculated transformation ratios for both the corrected and uncorrected temperatures indicate that the basal 300 m of the Monterey Formation has entered or is near the liquid oil window.

Discussion of Hydrocarbon Models

The maturity of the basal Monterey Formation as indicated by calculated transformation ratios is greater than that indicated by TTI calculations for two main reasons. First, as already discussed, the TTI method does not directly consider the type of kerogen present in the source rock. Instead, it uses average values of constants for all kerogen types. Thus, the TTI calculation tends to underestimate the thermal maturity of a relatively more easily degraded kerogen such as the type II kerogen as reported by Tissot and Espitalié (1975) or kerogen in the Phosphoria shale as reported by Lewan (1985). Second, the correlation of a TTI of 15 with the onset of oil generation is primarily based on general correlations with vitrinite reflectance,

Table 6. Activation Energies, Genetic Potential, and Hydrocarbon of Biochemical Origin for Type II Kerogen*

Class	Activation Energy		$A\ddagger$ (10^6 years) $^{-1}$
	Average Value (kcal mole $^{-1}$)	x_{i0} **	
E ₁₁	10	0.022	1.27×10^5
E ₁₂	30	0.034	7.47×10^{16}
E ₁₃	50	0.251	1.48×10^{27}
E ₁₄	60	0.152	5.52×10^{29}
E ₁₅	70	0.116	2.04×10^{35}
E ₁₆	80	0.120	3.80×10^{35}
Genetic potential of the kerogen (sum of x_{i0})			0.695
Hydrocarbon of biochemical origin (Y_0)			0.035

*From Tissot and Espitalié (1975).

** x_{i0} = genetic potential of kerogen class.

‡A = a rate constant. See text for discussion.

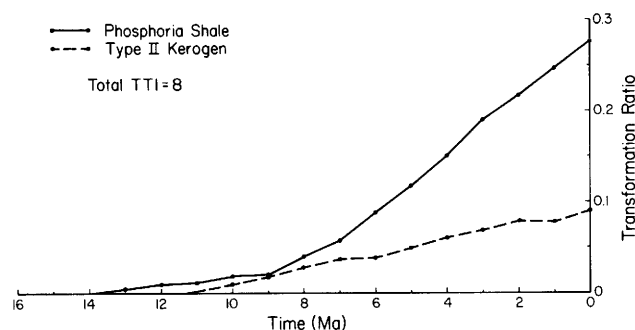


Figure 14—Results of maturation modeling for corrected temperature history of basal Monterey Formation in Pismo basin. Phosphoria shale kinetic values from Lewan (1985). Kinetic values for type II kerogen from Tissot and Espitalié (1975).

thermal alteration indices, and other maturation parameters. Such correlations may not be valid for an area, such as the Pismo basin, that has experienced drastic changes in its thermal and diagenetic histories.

IMPLICATIONS FOR HYDROCARBON EXPLORATION

The thermal and maturation models presented here indicate areas that have received larger and longer thermal pulses, which are: (1) basins closer to the Pacific-North American plate boundary, and (2) basins nearer the initial impingement of the ancestral East Pacific rise.

Factors that critically affect the maturation modeling are: (1) regional heat-flow through time; (2) kinetic properties of the source rocks; (3) depth of burial of the source rocks—for example, in the Pismo basin the basal Monterey Formation could be at peak oil generation if buried by an additional 300-900 m of Pismo Formation—and (4) the lithology, diagenesis, and compaction of both the source rock and the sediments that bury it. These factors significantly affect thermal conductivities and, hence, temperature histories of the sediments.

The thermal models developed in this paper demonstrate that hydrocarbon potential for coastal California basins must be evaluated in the context of regional geologic and thermal histories applied to specific basin details. Application of the models allows the evaluation of the maturation potential of the Monterey Formation in a dynamic time-temperature framework. This approach has important exploration implications relative to the Monterey Formation because it can evaluate maturation histories of a specific basin and make comparisons between different basins. Viewed in the context of this time-temperature framework, many of the apparent inconsistencies in the maturation of the Monterey Formation may be explained.

REFERENCES CITED

- Benfield, A. E., 1947, A heat-flow value for a well in California: *American Journal of Science*, v. 245, p. 1-18.
- Black, P. R., 1974, A quantitative test of a subduction model for observed heat-flow distributions in the western United States: Master's thesis, University of Wyoming, Laramie, Wyoming, 136 p.
- California Division of Oil and Gas, 1974, California oil and gas fields, v. 2, east-central California: Sacramento, State of California.
- Christensen, N. I., and M. H. Salisbury, 1975, Structure and constitution of the lower oceanic crust: *Reviews of Geophysics and Space Physics*, v. 13, p. 57-86.
- Crough, S. T., 1975, Thermal models of oceanic lithosphere: *Nature*, v. 256, p. 388-390.
- Dickinson, W. R., and W. S. Snyder, 1979a, Geometry of triple junctions related to San Andreas transform: *Journal of Geophysical Research*, v. 84, p. 561-572.
- , 1979b, Geometry of subducted slabs related to San Andreas transform: *Journal of Geology*, v. 87, p. 609-627.
- Erickson, A., 1973, Initial report on downhole temperature and shipboard thermal conductivity measurements, Leg 19, Deep Sea Drilling Project, in J. S. Creager, D. W. Scholl, et al., eds., *Initial Reports of the Deep Sea Drilling Project*, v. 19, p. 643-656.
- Furlong, K. P., 1984, Lithospheric behavior with triple junction migration: an example based on the Mendocino triple junction: *Physics of the Earth and Planetary Interiors*, v. 36, p. 213-223.
- , D. S. Chapman, and P. W. Alfeld, 1982, Thermal modeling of the geometry of subduction with implications for the tectonics of the overriding plate: *Journal of Geophysical Research*, v. 87, p. 1786-1802.
- Graham, S. A., and W. R. Dickinson, 1978, Evidence for 115 kilometers of right slip on the San Gregorio-Hosgri fault trend: *Science*, v. 199, p. 179-181.
- Hall, C. A., 1973a, Geology of the Arroyo Grande 15 minute quadrangle, San Luis Obispo County, California: California Division of Mines and Geology, Map Sheet 24.
- , 1973b, Geologic map of the Morro Bay south and Point San Luis quadrangles, San Luis Obispo County, California: USGS Miscellaneous Field Studies Map MF-511.
- , 1981, San Luis Obispo transform fault and middle Miocene rotation of the western Transverse Ranges, California: *Journal of Geophysical Research*, v. 86, p. 1015-1031.
- Heasler, H. P., 1984, Thermal evolution of coastal California with implications for hydrocarbon maturation: PhD thesis, University of Wyoming, Laramie, Wyoming, 76 p.
- , and R. C. Surdam, 1983, A thermally subsiding basin model for the maturation of hydrocarbons in Pismo basin, California, in C. M. Isaacs and R. E. Garrison, eds., *Petroleum generation and occurrence in the Miocene Monterey Formation, California: SEPM Pacific Section Special Publication*, p. 69-74.
- Hindmarsh, A. C., 1980, LODE: a computer program package for the solution of ordinary differential equations: Livermore, California, Lawrence Livermore Laboratory.
- Hunt, J. M., 1979, *Petroleum geochemistry and geology*: San Francisco, W. H. Freeman, 615 p.
- Isaacs, C. M., 1981, Porosity reduction during diagenesis of the Monterey Formation, Santa Barbara coastal area, California, in R. E. Garrison and R. G. Douglas, eds., *The Monterey Formation and related siliceous rocks of California: SEPM Pacific Section Special Publication*, p. 257-271.
- , 1983, Compositional variation and sequence in the Miocene Monterey Formation, Santa Barbara coastal area, California, in D. K. Larue and R. J. Steel, eds., *Cenozoic marine sedimentation, Pacific margin, USA: SEPM Pacific Section Special Publication*, p. 117-132.
- , 1984, The Monterey—key to offshore California boom: *Oil & Gas Journal*, v. 82 (January 9), p. 75-81.
- Kablanow, R. I., and R. C. Surdam, 1983, Diagenesis and hydrocarbon generation in the Monterey Formation, Huasna basin, California, in C. M. Isaacs and R. E. Garrison, eds., *Petroleum generation and occurrence in the Miocene Monterey Formation, California: SEPM Pacific Section Special Publication*, p. 53-68.
- Kilty, K., and D. S. Chapman, 1980, Convective heat transfer in selected geologic situations: *Groundwater*, v. 18, p. 386-394.
- Lachenbruch, A. H., 1968, Preliminary geothermal model of the Sierra Nevada: *Journal of Geophysical Research*, v. 73, p. 6977-6989.
- , and J. H. Sass, 1980, Heat flow and energetics of the San Andreas fault zone: *Journal of Geophysical Research*, v. 85, p. 6185-6223.
- Lewan, M. D., in press, Evaluation of petroleum generation by hydrous pyrolysis experimentation: *Philosophical Transactions of the Royal Society of London, Series A*.
- Murata, K. J., I. Friedman, and J. D. Gleason, 1977, Oxygen isotope relations between diagenetic silica minerals in the Monterey shale, Temblor Range, California: *American Journal of Science*, v. 277, p. 259-272.

- Orr, W. L., 1984, Sulfur and sulfur isotope ratios in Monterey oils of the Santa Maria River basin and Santa Barbara Channel area (abs.): SEPM Annual Midyear Meeting Abstracts, p. 62.
- Sass, J. H., A. H. Lachenbruch, R. J. Munroe, G. W. Greene, and T. H. Moses, 1971, Heat flow in the western United States: *Journal of Geophysical Research*, v. 76, p. 6376-6413.
- Stanley, K. O., and R. C. Surdam, 1984, The role of wrench fault tectonics and relative changes of sea level on deposition of upper Miocene-Pliocene Pismo Formation, Pismo syncline, California, in *Stratigraphic, tectonic, thermal, and diagenetic histories of the Monterey Formation, Pismo and Huasna basins, California*: SEPM Pacific Section Special Publication, p. 21-37.
- Steckler, M. S., and A. B. Watts, 1978, Subsidence of the Atlantic-type continental margin off New York: *Earth and Planetary Science Letters*, v. 41, p. 1-13.
- Surdam, R. C., and K. O. Stanley, 1981, Diagenesis and migration of hydrocarbons in the Monterey Formation, Pismo syncline, California, in R. E. Garrison and R. G. Douglas, eds., *The Monterey Formation and related siliceous rocks of California*: SEPM Pacific Section Special Publication, p. 317-327.
- Tissot, B. P., and J. Espitalié, 1975, Thermal evolution of organic matter in sediments: application of a mathematical simulation (in French): *Revue de l'Institut Français du Pétrole*, v. 30, p. 743-777.
- and D. H. Welte, 1978, *Petroleum formation and occurrence, a new approach to oil and gas exploration*: New York, Springer-Verlag, 538 p.
- Touloukian, Y. S., W. R. Judd, and R. F. Roy, eds., 1981, *Physical properties of rocks and minerals*: New York, McGraw-Hill, 548 p.
- Turcotte, D. L., and J. L. Ahern, 1977, On the thermal and subsidence history of sedimentary basins: *Journal of Geophysical Research*, v. 82, p. 3762-3766.
- and D. C. McAdoo, 1979, Thermal subsidence and petroleum generation in the southwestern block of the Los Angeles basin, California: *Journal of Geophysical Research*, v. 84, p. 3460-3464.
- and E. R. Oxburgh, 1969, Convection in a mantle with variable physical properties: *Journal of Geophysical Research*, v. 74, p. 1458-1474.
- Turner, D. L., 1970, Potassium-argon dating of Pacific coast Miocene foraminiferal stages: *GSA Special Paper 124*, p. 91-129.
- Wilson, J. T., 1965, A new class of faults and their bearing on continental drift: *Nature*, v. 201, p. 343-347.
- Waples, D., 1981, *Organic geochemistry for exploration geologist*: Minneapolis, Burgess, 151 p.
- Woodside, W., and J. H. Messmer, 1961, Thermal conductivity of porous media: *Journal of Applied Physics*, v. 32, p. 1688-1699.
- Zandt, G., and K. P. Furlong, 1982, Evolution and thickness of the lithosphere beneath coastal California: *Geology*, v. 10, p. 376-381.